Phase Transition of Short Linear Molecules Adsorbed on Solid Surfaces from a Density Functional Approach

P. Bryk*, K. Bucior, S. Sokołowski, and G. Żukociński

Department for the Modeling of Physico-Chemical Processes, Marie Curie-Skłodowska University, 20-031 Lublin, Poland

Received: July 15, 2004; In Final Form: November 15, 2004

A microscopic density functional theory is used to investigate the adsorption of short chains on strongly attractive solid surfaces. We analyze the structure of the adsorbed fluid and investigate how the layering transitions change with the change of the chain length and with relative strength of the fluid−solid interaction. The critical temperature of the first layering transition, rescaled by the bulk critical temperature, increases slightly with an increase of the chain length. We have found that for longer chains the layering transitions within consecutive layers are shifted toward very low temperatures and that their sequence is finally replaced by a single transition.

Introduction

Numerous density-functional-based approaches aiming at the description of nonuniform molecular fluids whose particles are built of a number of monomeric units have been proposed in the literature. One of the first such approaches was developed by Woodward[1,2] more than 10 years ago. Subsequently, Yethiraj and Woodward[3−5] proposed a theory based on a combination of a single-chain Monte Carlo simulation and a density-functional method. Another class of theories was based on the interaction site formalism.[6,7] One of the most interesting and important theories that have been developed recently extends Wertheim's thermodynamic perturbation theory[8] to the case of nonuniform chain fluids.[9,10] From a computational point of view, the approach by Yu and Wu[10,11] is particularly well suited to study the structure and thermodynamic properties of nonuniform fluids composed of tangentially bonded chains.

Previous density-functional-based studies of adsorption of chain particles have concentrated on models with repulsive forces only (cf. e.g., refs 1−3, 5, 7, 9, 10, 12, 13). In recent years theoretical effort has been shifted toward studies of the properties of bulk and nonuniform systems with attractive interparticle and particle-wall forces.[14−21] In particular, Müller et al.[16,18] reported the results of Monte Carlo, density-functional, and self-consistent field theory investigations of surface and interfacial properties of a molecular fluid composed of short linear chains (built of 10 segments). To describe the adsorbate molecules, they utilized a model of short polymer chains built of spherical sites connected by springs interacting with other sites and with the surface via Lennard-Jones-type potentials. Wertheim's thermodynamic perturbation theory was applied to describe connectivity of the segments. The developed approach reproduced the results of computer simulations with good accuracy. However, it also required much computational effort. Consequently, extensive studies of surface phase transitions within the framework of the theory of Müller et al.[18] would be rather time-consuming. In our opinion an attractive alternative for performing such studies is provided by the theory of Yu and Wu.[10,11]

In recent years there have also been reported numerous simulations of adsorption of alkanes on solid surfaces and in pores (see e.g. refs 22−28). These studies concentrated on an explanation of the molecular mechanism of some experimental observations, for example, anomalous crystallization in *n*-alkanes at the free surfaces[29] and phase behavior of layers of long-chain alkanes adsorbed at mica and metal surfaces[22,24] and between two solid surfaces.[23] Less attention has been paid to the investigation of vapor−liquid-phase equilibria of alkanes physisorbed on solids.[30,31] This is in part due to the fact that the experimental determination of the vapor−liquid phase diagrams of fluids adsorbed in monolayers is difficult.[32−35]

In our recent paper[36] we utilized the approach of Yu and Wu[10,11] to study the wetting transition in polymeric fluids consisting of short chains containing up to 10 homoatomic segments adsorbed on moderately adsorbing attractive walls. We observed that the wetting temperature rescaled by the bulk critical temperature decreased with an increase of the chain length. For longer chains this temperature reached a plateau. For the surface critical temperature an inverse effect was observed; that is, the surface critical temperature increased with the chain length and then attained a plateau.

It is well-known that in the case of adsorption of atomic fluids on strongly adsorbing surfaces a sequence of layering-type transitions may appear.[37] Layering near the liquid−solid interface has also been demonstrated experimentally.[38,39] This phenomenon has been observed both in fluids of spherical particles and in chain fluids. For example, Winkler et al.[40] compared the layering in the case of adsorption of liquid hexadecane in contact on a model corrugated graphite surface with adsorption on a model purely repulsive flat surface. Gupta et al.[41] investigated the structure and dynamics of liquid octane adsorbed on a series of corrugated Lennard-Jones surfaces with varying degree of attraction for the liquid.

Moreover, Smith et al.[25] found layering during investigations of adsorption of butane, octane, and their mixtures on a wax-like substrate. No hints of frozen layers even near the bulk freezing temperature were found.

To our best knowledge, there are no studies reporting the surface phase diagrams for adsorbed chain particles, which

* Corresponding author. E-mail: pawel@paco.umcs.lublin.pl.

10.1021/jp0468511 CCC: $30.25
Published on Web 01/20/2005

include several layering transitons. Computer simulations carried out so far focused on the phase behavior within a single layer adjacent to the adsorbing surface, cf. refs 30 and 31. Thus, the principal aim of this work is to evaluate phase diagrams for a sequence of layering transitions in the case of adsorption of short chains, built of up to 8 segments. We apply the density-functional theory of Yu and Wu[10,11] and a mean-field approximation to calculate the contribution to the free energy functional arising from attractive segment−segment interaction. Because of a mean-field type of theory we do not expect our theoretical predictions to remain in quantitative agreement with computer simulations. However, we can expect that a general picture of the phase transitions in such systems should be correctly predicted at a qualitative level.

Theory

The theory outlined below describes thermodynamic and structural properties of a fluid composed of chain particles in contact with an impenetrable solid surface. According to the adopted model, each particle of the fluid is built of M spherical segments, which are tangentially joined by a bonding potential acting between the adjacent segments of the same chain. In principle, the theory can be easily written for a quite general case of segments of different sizes. However, we restrict our considerations to the case of segments of identical diameters σ. The diameter σ determines the segment hard core, and any overlap between two segments is forbidden.[10,13]

The total bonding potential, $V_b(\mathbf{R})$, is a sum of bonding potentials υ_b between the adjacent segments:

$$V_b(\mathbf{R}) = \sum_{j=1}^{M-1} \upsilon_b(|\mathbf{r}_{j+1} - \mathbf{r}_j|) \tag{1}$$

In the above $\mathbf{R} \equiv (\mathbf{r}_1,\mathbf{r}_2,\cdots,\mathbf{r}_M)$ denotes a set of coordinates of the segment positions. This potential satisfies the relation

$$\exp[-\beta V_b(\mathbf{R})] = \prod_{j=1}^{M-1} \delta(|\mathbf{r}_{j+1} - \mathbf{r}_j| - \sigma)/4\pi\sigma^2 \tag{2}$$

In addition to the hard-sphere and to the bonding potential there also exists an attractive interaction between all the segments. We assume that the attractive van der Waals potential has the form

$$u(r) = \begin{bmatrix} 0 & \text{for } r \le \sigma, \\ 4\epsilon[(\sigma/r)^{12} - (\sigma/r)^6] & \text{for } \sigma < r \le r_{cut} \\ 0 & \text{for } r > r_{cut}, \end{bmatrix} \tag{3}$$

where r_{cut} is the cutoff distance and ϵ is the energy parameter. The latter parameter is assumed to be independent of the interacting segment index. The form of the potential (eq 3) excludes the interaction between the adjacent segments within the same chain.

The fluid is in contact with a solid surface, and each segment j interacts with the surface via a Lennard-Jones (9−3) potential:

$$\upsilon_j(z_j) = \epsilon_{gs}[(z_0/z_j)^9 - (z_0/z_j)^3] \tag{4}$$

where z_j is the distance between the jth segment and the surface. The parameters ϵ_{gs} and z_0 are identical for all segments. The total external potential, $V_{ext}(\mathbf{R})$, for a chain molecule is assumed to be a sum of the external potential energies imposed on individual segments:

$$V_{ext}(\mathbf{R}) = \sum_{j=1}^{M} \upsilon_j(\mathbf{r}_j) \tag{5}$$

We note here that the model described above differs from those applied in refs 16−19. The principal difference results from the fact that in our approach we assume that the bonding potential, υ_b, is of infinitely short range, whereas in the above cited publications the so-called finitely extensible nonlinear elastic potential, responsible for the connectivity between the adjacent segments, has been used.

As we have already mentioned, the density-functional approach employed to describe the system is based on the theory of Yu and Wu.[10] In this approach the grand potential of the system Ω is assumed to be a functional of the local density of the fluid, $\rho(\mathbf{R})$,

$$\Omega[\rho(\mathbf{R})] = F_{id}[\rho(\mathbf{R})] + F_{ex}[\rho(\mathbf{R})] + \int d\mathbf{R}\rho(\mathbf{R})(V_{ext}(\mathbf{R}) - \mu) + F_{att}[\rho(\mathbf{R})] \tag{6}$$

where μ is the chemical potential, F_{id} defined as

$$\beta F_{id}[\rho(\mathbf{R})] = \beta\int d\mathbf{R}\rho(\mathbf{R})V_b(\mathbf{R}) + \int d\mathbf{R}\rho(\mathbf{R})[\ln(\rho(\mathbf{R})) - 1] \tag{7}$$

is the ideal configurational part of the free energy, F_{ex} is the excess free energy of hard-sphere chains, and F_{att} is the free energy due to attractive forces between the particles.

The contribution F_{ex} can be split into the hard-sphere contribution, F_{HS}, which results from the hard-sphere repulsion between segments, and the contribution due to chain connectivity, F_C. Each of the contributions is a functional of the average segment density defined as

$$\rho_s(\mathbf{r}) = \sum_{j=1}^{M} \rho_{s,j}(\mathbf{r}) = \sum_{j=1}^{M} \int d\mathbf{R}\delta(\mathbf{r} - \mathbf{r}_j)\rho(\mathbf{R}) \tag{8}$$

where $\rho_{s,j}(\mathbf{r})$ is the local density of the segment j of the chain. Each of the components, F_α, $\alpha = HS$ or C, is expressed as a volume integral $F_\alpha = \int\Phi_\alpha(\mathbf{r})d\mathbf{r}$.

The hard-sphere contribution is evaluated from the fundamental measure theory[42−44]

$$\Phi_{HS} = -n_0\ln(1 - n_3) + \frac{n_1n_2 - \mathbf{n}\cdot\mathbf{n}_2}{1 - n_3} + n_2^3(1 - \xi^2)^3\frac{n_3 + (1 - n_3)^2\ln(1 - n_3)}{36\pi n_3^2(1 - n_3)^2} \tag{9}$$

where $\xi(\mathbf{r}) = |\mathbf{n}_2(\mathbf{r})|/n_2(\mathbf{r})$.

The contribution Φ_C is obtained from Wertheim's first-order perturbation theory:[8]

$$\Phi_C = \frac{1 - M}{M} n_0\zeta\ln[y_{HS}(\sigma)] \tag{10}$$

where $\zeta = 1 - \mathbf{n}_{V2}\cdot\mathbf{n}_{V2}/(n_2)^2$ and the contact value of the hard-sphere radial distribution function, y_{HS}, results from Carnahan−Starling equation of state:

$$y_{HS}(\sigma) = \frac{1}{1 - n_3} + \frac{n_2\sigma\zeta}{4(1 - n_3)^2} + \frac{(n_2\sigma)^2\zeta}{72(1 - n_3)^3} \tag{11}$$

In the above $\zeta = 1 - \mathbf{n}_{V2}\cdot\mathbf{n}_{V2}/(n_2)^2$ and n_α, $\alpha = 0, 1, 2, 3, V1,$

$V2$, are the weighted densities,

$$n_\alpha(\mathbf{r}) = \int d\mathbf{r}' \rho_s(\mathbf{r}') w_\alpha(\mathbf{r} - \mathbf{r}') \quad (12)$$

where the weight functions $w_\alpha(\mathbf{r})$ are given in ref 42.

Finally, we write the mean-field attractive potential contribution to the free-energy:

$$F_{att} = \frac{1}{2}\int d\mathbf{r}d\mathbf{r}' u(|\mathbf{r} - \mathbf{r}'|)\rho_s(\mathbf{r})\rho_s(\mathbf{r}') \quad (13)$$

We stress that the last equation is valid if all the segments are identical.

The equilibrium density profile $\rho(\mathbf{R})$ is determined minimizing the grand potential, i.e., from the condition $\delta\Omega[\rho(\mathbf{R})]/\delta\rho(\mathbf{R}) = 0$. Thus

$$\rho(\mathbf{R}) = \exp\{\beta\mu - \beta V_b(\mathbf{R}) - \beta \sum_{j=1, M} \lambda_j(\mathbf{r}_j)\} \quad (14)$$

where $\lambda_j(\mathbf{r}_j)$ is

$$\lambda_j(\mathbf{r}_j) = \frac{\delta[F_{ex} + F_{att}]}{\delta\rho_s(\mathbf{r}_j)} + v_j(\mathbf{r}_j) \quad (15)$$

From the last equation and eq 8 we obtain final equation for the average segment local density:

$$\rho_s(\mathbf{r}) = \exp(\beta\mu)\int d\mathbf{R}\sum_{j=1}^{M}\delta(\mathbf{r} - \mathbf{r}_j)\exp[-\beta V_b(\mathbf{R}) - \beta\sum_{l=1}^{M}\lambda_l(\mathbf{r}_l)] \quad (16)$$

For the present case of the planar symmetry eq 16 can be rewritten as

$$\rho_s(z) = \exp(\beta\mu)\sum_{j=1}^{M}\exp[-\beta\lambda_j(z)]G_j(z)G_{M+1-j}(z) \quad (17)$$

where the propagator function $G_j(z)$ is determined from the recurrence relation

$$G_j(z) = \begin{bmatrix} 1 & \text{for } j = 1 \\ \int dz' \exp[-\beta\lambda_j(z')]\dfrac{\theta(\sigma - |z - z'|)}{2\sigma} G_{j-1}(z') & \text{for } 1 < j < M \end{bmatrix} \quad (18)$$

where θ is the step function.

Results and Discussion

We report the results for the systems containing molecules built of $M = 2$, 4, and 8 segments. Because we are interested in the studies of adsorption from a gaseous phase, the calculations have been preceded by the evaluation of the bulk phase diagrams. This has been done by means of a bulk counterpart of the theory outlined above. The relevant equations can be easily written setting the local density to be constant and equal to the bulk density.

In Figure 1 we show examples of the liquid−vapor coexistence envelopes in the reduced bulk segment density $\rho_b^* = \rho_{s,b}\sigma^3$ − reduced temperature $T^* = k_BT/\epsilon$ plane for the chains of length $M = 2$, 4, and 8. To make the dependence of the vapor density on temperature more transparent, we have used logarithmic density scale. The location of the critical points is marked by diamonds. Note that all our calculations have been carried out assuming the cutoff distance $r_{cut} = 3\sigma$.

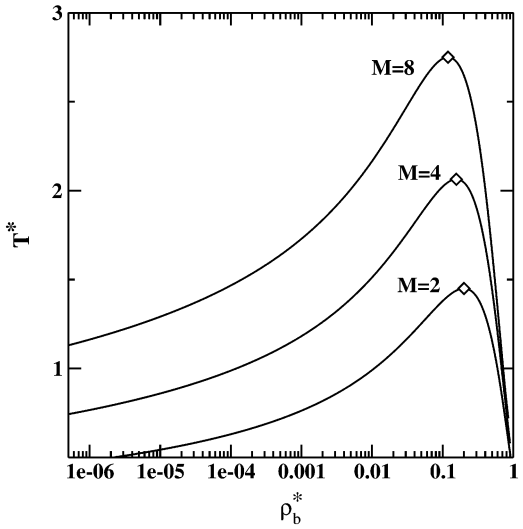

Figure 1. Liquid−vapor phase diagrams of dimers, tetramers, and octamers in the density−temperature plane. Critical points are marked by diamonds.

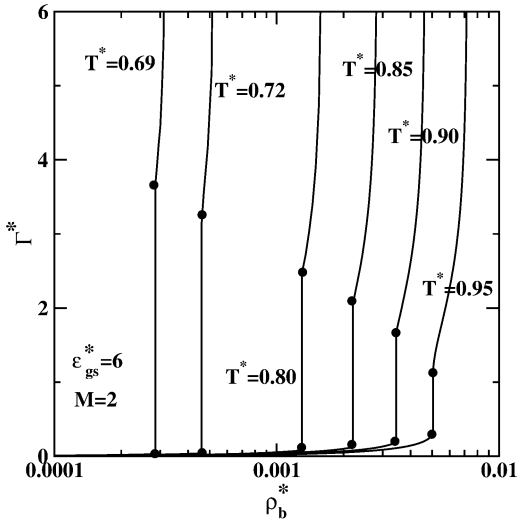

Figure 2. Series of adsorption isotherms of dimers, $\Gamma^* = \Gamma\sigma^2$, on the surface characterized by $\epsilon_{gs}^* = \epsilon_{gs}/\epsilon = 6$ at different temperatures marked in the figure. Black points indicate the prewetting jumps.

We now proceed to the presentation of the results of adsorption. For a given value of M we first solve the density profile eq 17 and then evaluate the "segment adsorption isotherm"

$$\Gamma = \int_0^\infty dz[\rho_s(z) - \rho_{s,b}] \quad (19)$$

and the excess grand potential $\Delta\Omega = \Omega - \Omega_b$, where Ω_b is the grand potential of a uniform fluid being in equilibrium with the nonuniform system. The analysis of the dependence of $\Delta\Omega$ on the chemical potential allows for a precise location of the surface phase transitions.

In Figure 2 we show examples of the adsorption isotherms of dimers on a moderately adsorbing surface, $\epsilon_{gs}^* = \epsilon_{gs}/\epsilon = 6$. At the reduced temperatures $T^* > 0.63$ this system exhibits a typical wetting transitions; that is, at $T^* \le T_w^* \approx 0.63$ only a thin film is formed at the surface, whereas at temperatures higher than the wetting temperature, T_w, the adsorption isotherms di-

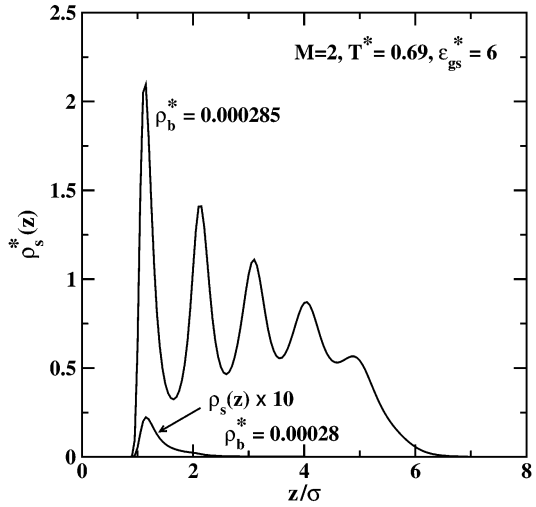

Figure 3. Example of the film thickness change during prewetting transition. To make the profile for the thin film visible, the values of the local density have been multiplied by 10. All the parameters are given in the figure.

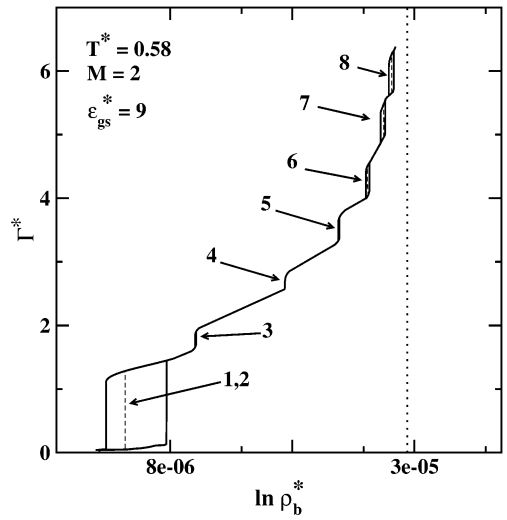

Figure 4. Adsorption isotherm of dimers on the surface $\epsilon^*_{gs} = 9$ at $T^* = 0.58$. Each step is marked by a label indicating the layer number. The equilibrium transitions are indicated by vertical dashed lines. The metastable states within the consecutive van der Waals loops are marked by solid lines, whereas the dotted line marks the bulk gas−liquid transition.

verge on approaching the bulk liquid−vapor coexistence density. Moreover, at temperatures lower than the surface critical temperature, $T^*_{sc} \approx 0.975$, the fluid exhibits a first-order prewetting transition manifested by a discontinuity on the adsorption isotherm. Black circles in Figure 2 mark the end of the prewetting jump.

Figure 3 illustrates the change of the film thickness upon the prewetting transition. The profiles displayed here are for the temperature close to the wetting temperature. The density profile before the prewetting transition indicates that only one incompletely filled layer is formed, whereas the thick film extends over five layers.

If the adsorbing surface becomes more attractive, $\epsilon^*_{gs} = 9$, the scenario of surface phase transitions is altered. In Figure 4 we show an example of the adsorption−desorption isotherm of dimers at a quite low temperature, $T^* = 0.58$. The adsorption exhibits a series of well-pronounced steps, seven of which are displayed in the figure. However, the first step corresponds to

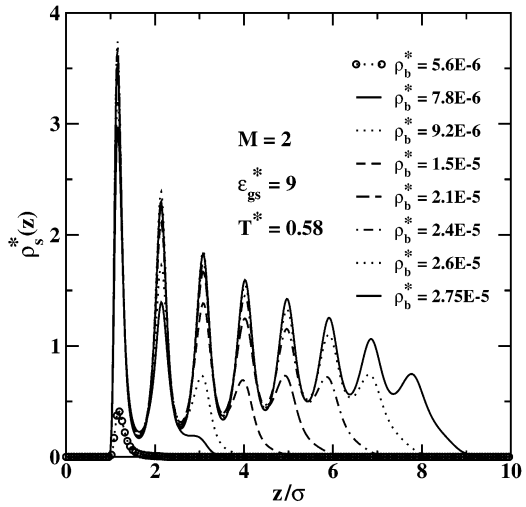

Figure 5. Average segment density profiles after each layering transition and the density profile before the first transition (dotted line with circles). All the parameters are given in the figure.

an instantaneous filling of the first two layers adjacent to the pore wall. For the density approaching the bulk dew density (marked by the dotted vertical line in Figure 4) consecutive steps appear in adsorption isotherm. However, they are located closer and closer to the bulk coexistence and their precise location is more and more difficult. For this reason we have limited ourselves to the investigation of the sequence of the first eight layering transitions only. Each step corresponds to the layering transition. Vertical dashed lines locate the bulk densities at which the thermodynamic equilibrium between two states occurs; they have been evaluated analyzing the dependence of the excess grand potentials on the chemical potential.

The question regarding the character of each transition can be answered inspecting the density profiles, cf. Figure 5. We see that the first step is associated with the layering transition, which takes place within the first two layers. The next transitions occur within single consecutive layers. It would be of interest to investigate the arrangement of the chains within a layer and in particular to check the orientation of the chain backbones with respect to the substrate. Unfortunately, within our approach it is not possible to address these issues.

The resulting phase diagram is displayed in Figure 6. The calculations have been carried out for several temperatures $T^* \geq 0.55$. Lower temperatures have not been investigated due to the onset of the freezing transition. Figure 6a shows the diagram in the adsorption−temperature plane. There are two temperature scales. The left-hand temperature axis uses the usual reduced temperature, whereas the right-hand axis gives the temperature reduced by the bulk critical temperature. The latter is equal to 1.4499 for the dimers.

The phase diagram in Figure 6a is composed of several branches; each of them is associated with the relevant layering transition. At temperatures higher than approximately 0.6095 the first branch divides into two, each of them corresponding to the layering within a single adlayer. At lower temperatures these two branches merge into one. The temperature 0.6095 is thus the triple-point temperature. As we have already mentioned, we refrained from calculations at very low temperatures, and therefore the question of the existence of the triple points between next layering transitions remains open. The critical temperature of the layering transition is a non-monotonic function of the layer number and attains a minimum for the transition within the fourth layer.

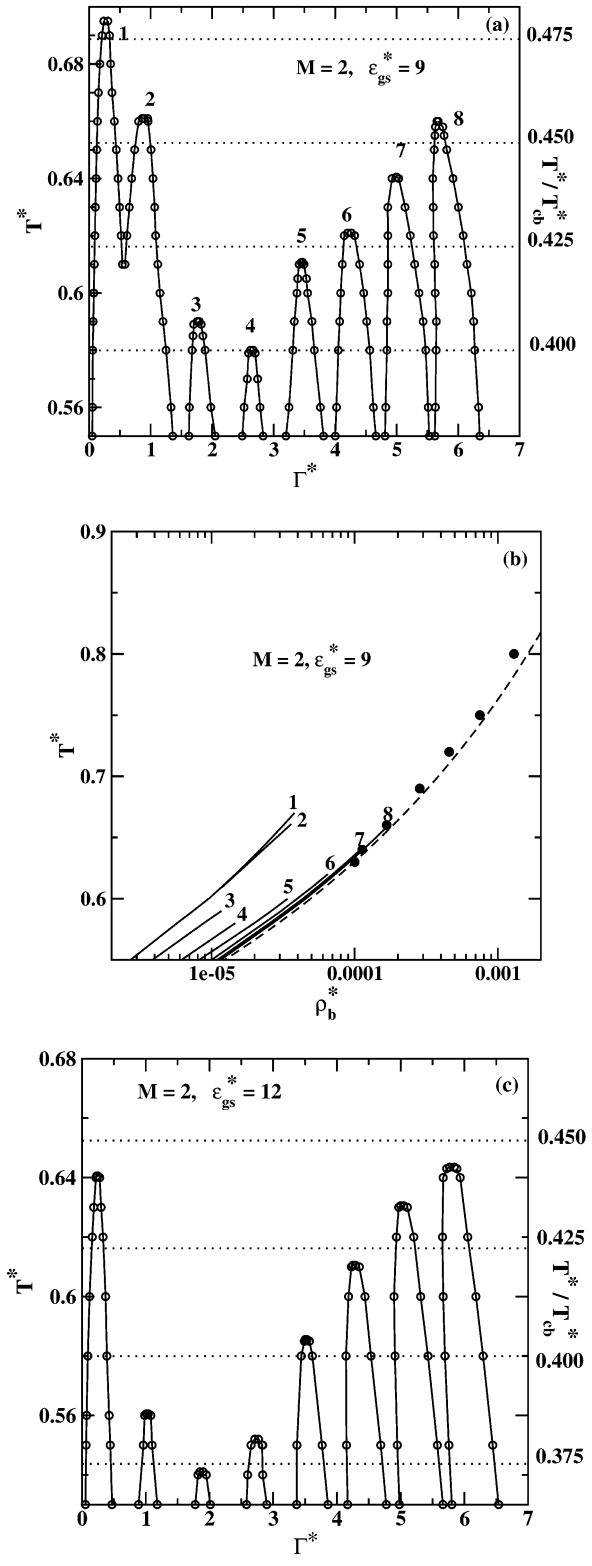

Figure 6. Phase diagrams for the system with $M = 2$ and $\epsilon_{gs} = 9$. Part a shows the diagram in the adsorption−temperature plane. Right-hand temperature axis shows the temperature reduced by the bulk critical temperature. The numbers denote the consecutive layering transitions. Part b shows the same phase diagram, but in the bulk density−temperature plane. The prewetting line for the system with $\epsilon_{gs} = 6$ is marked by black dots, whereas the dashed line denotes the bulk dew line. Part c shows the phase diagram for the system with $M = 2$ and $\epsilon_{gs} = 12$.

Part b of Figure 6 shows the diagram in the bulk density−the temperature plane. The numbers in both parts of Figure 6 refer to the respective layering transitions. We also show here the vapor branch of the bulk phase diagram and the prewetting line for the system with $\epsilon_{gs} = 6$. It is evident that the layering transitions for the further layers lie extremely close to the coexistence.

The phase diagram for the dimers adsorbed on still more attractive surface, $\epsilon^*_{gs} = 12$, is shown in Figure 6c. Its shape is qualitatively similar to that for $\epsilon^*_{gs} = 9$. However, the critical and triple-point temperatures for the corresponding layering transitions become lower because an increase of the adsorption energy causes the adlayers to become more "compact", two-dimensional. The critical temperature attains a minimum for the third layer. Note also that the critical temperature of the transition within the eight layer is now slightly higher than the corresponding critical temperature for the first layering.

The results presented so far can be summarized as follows. For $\epsilon^*_{gs} = 6$ we observe a prewetting transition, i.e., instantaneous filling of several adlayers, whereas for $\epsilon^*_{gs} = 9$ and 12 the phase diagrams exhibit a sequence of layering transitions. Thus, for $6 < \epsilon^*_{gs} < 9$ there must be a crossover between both these scenarios of phase transformations. Indeed, performing some additional calculations for $\epsilon^*_{gs} = 8$ (not shown) we have found that for $T^* < 0.56$ the first layering transition occurs within three layers and there is no triple point between the transitions within the first and the second layering transition. There exists, however, a triple point between the second and the third layering transitions, and a rough estimate gives a temperature range between 0.56 and 0.58. We can thus expect that further decrease of the fluid−wall attraction should result in merging the next layering transitions.

Figure 7a is a counterpart of Figure 6a and Figure 7b is a counterpart of Figure 6c, but now the results are for $M = 4$. The identification of particular branches follows from the inspection of the density profiles (for the sake of brevity, we do not show them here). Comparing the diagram for dimers (Figure 6) and for tetramers (Figure 7) adsorbed on the same surface we find the following differences. The first branch for tetramers describes the transition within the first two layers adjacent to the wall. Unlike the case of dimers, this branch of the phase diagram for tetramers does not divide into two parts at higher temperatures and there is no corresponding triple point. However, we observe the triple point between this branch and that for the transition within the third layer. For the system $\epsilon^*_{gs} = 9$ this triple-point temperature is between between 0.58 and 0.6. The critical temperatures for the layering transitions within the third and the next layers are now significantly lower than the first layering critical temperature. For $\epsilon^*_{gs} = 12$ the critical temperatures of the third and consecutive layering transitions are quite low; indeed, they are lower than 0.35 of the bulk critical temperature. The estimated value of critical temperature, T^*_{cb}, of the layering within the third layer is about $0.28T^*_{cb}$. We also note that for $\epsilon^*_{gs} = 6$ the adsorbed tetramers exhibit the wetting transition with the reduced wetting and surface critical temperatures equal to 0.705 and 1.415, respectively.[36]

Finally, we discuss the results for $M = 8$. For both values of $\epsilon^*_{gs} = 9$ and 12 for the temperatures $T^*/T^*_{cb} < 0.3$ (note that the bulk critical temperature for octamers equals 2.7504538) we observe only a single layering transition at quite low bulk densities or a continuous film growth. Consecutive layerings, if they exist, would appear at reduced temperatures significantly lower than $T^* < 0.65$.

An example of the adsorption isotherm of octamers is displayed in Figure 8. The first step of the isotherm (marked "1") appears at very low bulk densities. We also find that the

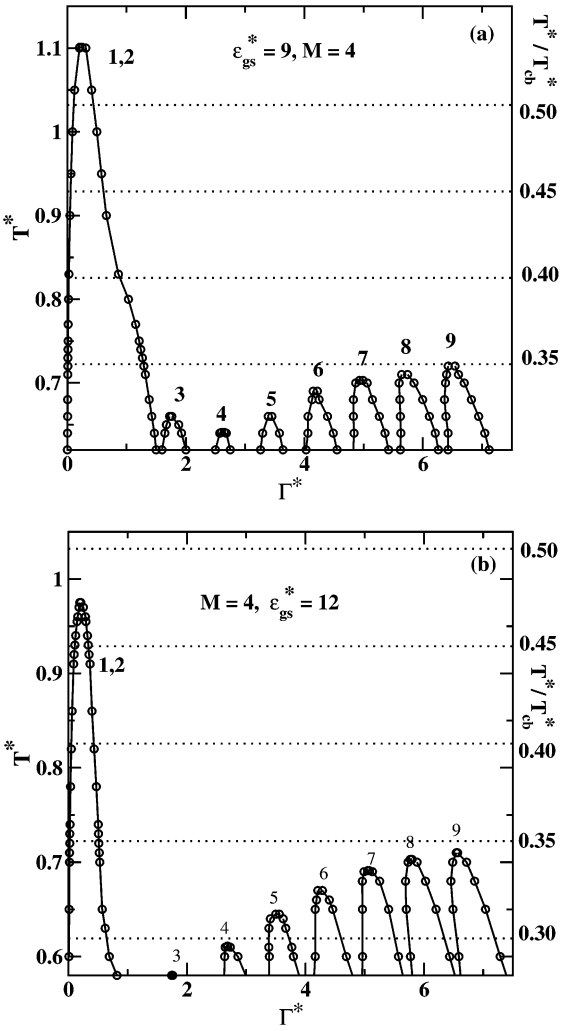

Figure 7. Phase diagrams for the system with $M = 4$ in the adsorption−temperature plane. Right-hand temperature axis shows the temperature reduced by the bulk critical temperature. The numbers denote the consecutive layering transitions. Part a is for $\epsilon_{gs} = 9$, whereas part b is for $\epsilon_{gs} = 12$.

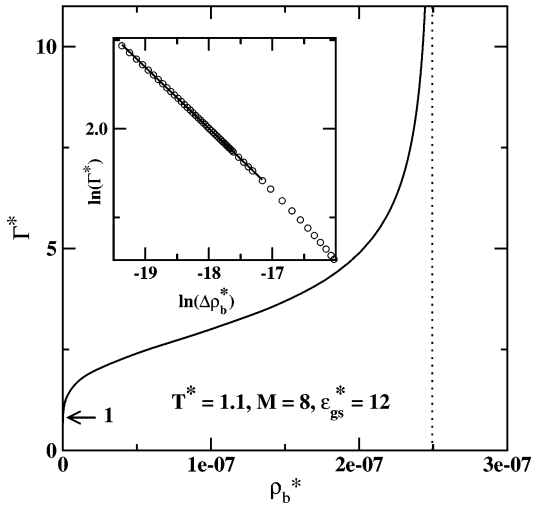

Figure 8. Example of the adsorption isotherm of octamers. The position of the first step is indicated by the label "1". The inset shows the log−log plot of the adsorption isotherm. Here $\Delta\rho_b^* = \rho_{bc}^* - \rho_b^*$, where ρ_{bc}^* is the gas segment density at bulk coexistence.

adsorption divergence upon approaching the bulk coexistence is a power law, i.e., $\Gamma^* \propto (\rho_{bc}^* - \rho_b^*)^{-1/3}$, where ρ_{bc} is the gas

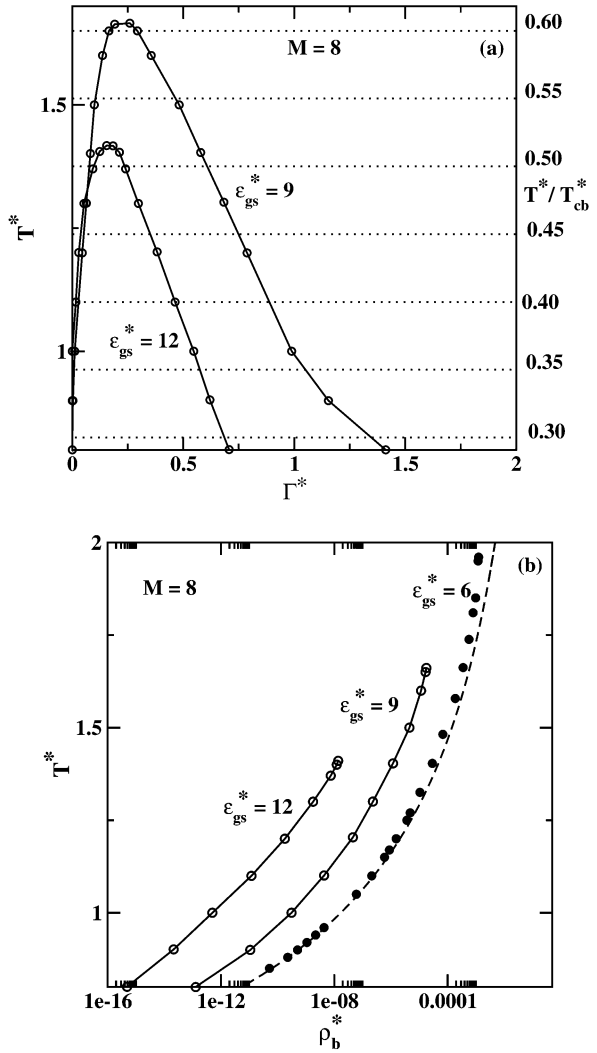

Figure 9. Phase diagrams for the system with $M = 8$. Part a shows the diagram in the adsorption−temperature plane. Right-hand vertical axis is for the temperature reduced by the bulk critical temperature. The latter temperature is 2.7504538. There is only one transition for $\epsilon_{gs}^* = 9$, as well as for $\epsilon_{gs}^* = 12$. Part b shows the phase diagrams in the bulk density−temperature plane. Additionally we display here the prewetting line (black dots) for the system with $\epsilon_{gs}^* = 6$ and the bulk dew line (dashed line).

segment density at bulk coexistence ($\rho_{bc} = 2.4937382 \times 10^{-7}$ at $T^* = 1.1$). This behavior is clearly visible on the log−log plot of adsorption where the straight line slope equals −1/3. The same behavior has been observed for all the systems under study and is characteristic for the complete wetting regime in systems with long-range fluid−fluid and/or fluid−solid potentials.[45,46]

The surface phase diagrams evaluated for 8-mers are plotted in Figure 9. Part a gives the diagrams in the adsorption−temperature plane, whereas part b, in the bulk segment density−temperature plane. As we have already emphasized for both values of $\epsilon_{gs}^* = 9$ and 12 we observe only a single transition within the layer adjacent to the pore wall. After this transition the film growth is continuous.

In Figure 9b we have also marked the prewetting line for the system with moderately adsorbing potential, $\epsilon_{gs}^* = 6$. The prewetting line (black circles) joins the binodal (dashed line) tangentially at the wetting temperature and ends at the surface critical temperature. The reduced wetting temperature T_w^* is 0.845, and the surface critical temperature T_{sc}^* equals 1.965.

However the film morphology for the prewetting transition is different from that for the layering transition. For $\epsilon^*_{gs} = 6$ and at the temperature close to the wetting temperature the prewetting transition is between the almost completely empty first layer and a thick film extending over more than six layers. At temperatures close to the surface critical temperature the thickness of the film directly after the prewetting transition is smaller, and for example, at $T^* = 1.85$ this film spans over approximately three layers.[36]

Summary

We have carried out studies of surface phase transitions in the case of adsorption of fluids composed of chains built of two, four, and eight freely jointed tangent Lennard-Jones monomers. The difference in the chain lengths leads to differences in the surface phase behavior. Considering adsorption on surfaces characterized by the same value of ϵ^*_{gs} we have found that the critical temperature of the first layering transition, T_{l1}, rescaled by the bulk critical temperature, increases slightly with an increase of the chain length. For the strongest surface-segment potential, $\epsilon^*_{gs} = 12$, the ratio $T^*_{l1}/T^*_{cb} \approx 0.44$ for dimers, 0.4 for 4-mers, and 0.51 for 8-mers. Note that the experimental value for of T^*_{l1}/T^*_{cb} is $\sim$0.43 for ethane film adsorbed on graphite.[35]

In a recently published work Potoff and Siepmann[31] used histogram-reweighting Monte Carlo simulations in the grand canonical ensemble to study adsorption of a series of alkanes on a flat gold surface. They found that the ratio of the two-dimensional to the three-dimensional (bulk) critical temperatures depended weakly on the chain length and decreased from 0.38 for methane to 0.31 for *n*-decane. This result contrasts with our findings. We attribute these differences to the fact that in the model used by Pottoff and Siepmann[31] the segments are separated by bonds of length equal to about 0.4 σ. Therefore, the segment packing density at the surface is much higher when the alkanes adsorb with their backbones parallel to the substrate. However in the model considered in our study the segments are connected tangentially (bond length equal to σ). Therefore it is much more likely for some chains to extend away from the surface. This promotes the adsorption of multiple layers and may lead to an instantaneous condensation within one, two, or even three adlayers, as for example for $M = 2$ and $\epsilon^*_{gs} = 8$. Within this context it is not surprising that the ratios of the critical temperatures in the present study are somewhat higher.

The critical temperatures of the layering transitions within the consecutive layers, rescaled by the bulk critical temperature, decrease with an increase of the chain length. Indeed, in the case of the longest chains investigated in this work, $M = 8$, the critical temperatures of all layering transitions but the first one are below the range of the temperatures studied. It is thus possible that for $M = 8$ we do, in fact, observe only a prewetting-type transition, and the envelope displayed in Figure 9 describes a high-temperature part of the prewetting diagram. We conclude that for longer chains the layering-type transition are shifted toward lower and lower temperatures, and consequently, for long enough chains only the wetting transition is preserved.

In this paper we do not consider the onset of the freezing transition. However, in a recent study Vega et al.[47] determined the global bulk phase diagram of tangentially bonded Lennard-Jones chains. They found that the triple-point temperature decreases with the chain length increase, tending for large M to an asymptotic value of $T^*_t(M \rightarrow \infty) = 0.634$. Although these authors used a different formula for the contact value of the radial distribution function of the monomers, this value suggests that within our approach some of the layering transitions are metastable with respect to a broader vapor−solid transition. This should lead to even more interesting surface phase diagrams, as for example from Figure 6a only the first, second, and eight layering transition would prevail. On the other hand, an incorporation of the bending and torsional potentials into the model will dramatically alter the global phase diagram of the underlying chain fluid. Therefore, we postpone a detailed investigation this problem for future work. The possibility of application of the present theory to the study of wetting-type behavior of adsorbed long-chain particles is currently under study in our laboratory.

Acknowledgment. P.B. acknowledges financial support from the Rector of the Marie Curie-Skl odowska University, Lublin. S.S. acknowledges the EU for partially funding this work as TOK contract 509249.

References and Notes

(1) Woodward, C. E. *J. Chem. Phys.* **1991**, *94*, 3138.
(2) Woodward, C. E. *J. Chem. Phys.* **1992**, *97*, 4525.
(3) Yethiraj, A.; Woodward, C. E. *J. Chem. Phys.* **1995**, *102*, 5499.
(4) Yethiraj, A. *J. Chem. Phys.* **1998**, *109*, 3269.
(5) Yethiraj, A. *Adv. Chem. Phys.* **2002**, *112*, 82.
(6) Chandler, D.; McCoy, J. D.; Singer, S. J. *J. Chem. Phys.* **1986**, *85*, 5971.
(7) Hooper, J. B.; McCoy, J. D.; Curro, J. G. *J. Chem. Phys.* **2000**, *112*, 3090.
(8) Wertheim, M. S. *J. Chem. Phys.* **1987**, *87*, 7323.
(9) Kierlik, E.; Rosinberg, M. L. *J. Chem. Phys.* **1992**, *97*, 9222.
(10) Yu, Y.-X.; Wu, J. *J. Chem. Phys.* **2002**, *117*, 2368.
(11) Yu, Y.-X.; Wu, J. *J. Chem. Phys.* **2003**, *118*, 3835.
(12) Cai, J.; Liu, H.; Hu, Y. *Fluid Phase Equilibria* **2002**, *194*, 282.
(13) Bryk, P.; Sokol owski, S. *J. Chem. Phys.* **2004**, *120*, 8299.
(14) Patra, C. N.; Yethiraj, A. *J. Chem. Phys.* **2000**, *112*, 1579.
(15) Patra, C. N.; Yethiraj, A. *J. Chem. Phys.* **2003**, *118*, 4702.
(16) Müller, M.; MacDowell, L. G. *Macromolecules* **2000**, *33*, 3902.
(17) Müller, M.; MacDowell, L. G.; Müller-Buschbaum, P.; Wunnike, O.; Stamm, M. *J. Chem. Phys.* **2001**, *115*, 9960.
(18) Müller, M.; MacDowell, L. G.; Yethiraj, A. *J. Chem. Phys.* **2003**, *118*, 2929.
(19) MacDowell, L. G.; Müller, M.; Vega, C.; Binder, K. *J. Chem. Phys.* **2000**, *113*, 419.
(20) Zhang, S.; Cai, J.; Liu, H.; Hu, Y. *Mol. Simulat.* **2004**, *30*, 143.
(21) Wang, X.-Y.; Chiew, Y. C. *J. Chem. Phys.* **2001**, *115*, 4376.
(22) Balasubramanian, S.; Klein, M. L.; Siepmann, J. I. *J. Chem. Phys.* **1995**, *103*, 3184.
(23) Dijkstra, M. *J. Chem. Phys.* **1997**, *107*, 3277.
(24) Dijkstra, M. *Thin Solid Films* **1998**, *330*, 14.
(25) Smith, P.; Lynden-Bell, R. M.; Smith, W. *Mol. Phys.* **2000**, *98*, 255.
(26) Shimizu, T.; Yamamoto, T. *J. Chem. Phys.* **2000**, *113*, 3351.
(27) Li, H. Z.; Yamamoto, T. *J. Chem. Phys.* **2001**, *114*, 5774.
(28) Li, H. Z.; Yamamoto, T. *J. Phys. Soc. Jpn.* **2002**, *71*, 1083.
(29) Maeda, N.; Kohonen, M. M.; Christenson, H. K. *J. Phys. Chem. B* **2001**, *105*, 5906.
(30) Potoff, J. J.; Siepmann, J. I. *Phys. Rev. Lett.* **2000**, *85*, 3460.
(31) Potoff, J. J.; Siepmann, J. I. *Langmuir* **2002**, *18*, 6088.
(32) Kim, H. K.; Chan, M. H. W. *Phys. Rev. Lett.* **1984**, *53*, 170.
(33) Regnier, J.; Menaucourt, J.; Thomy, A.; Duval, X. *J. Chem. Phys.* **1981**, *78*, 629.
(34) Poirier, G.; Fitts, W. P.; White, J. M. *Langmuir* **2001**, *17*, 1176.
(35) Steele, W. A. *Langmuir* **1996**, *12*, 145.
(36) Bryk, P.; Sokołowski, S. *J. Chem. Phys.* **2004**, *121*, 11314.
(37) Evans, R.; de Carvalho, R. J. F. L. *Am. Chem. Soc. Symp. Ser.* **1996**, *629*, 166−184.
(38) O'Shea, S. J.; Welland, M. E.; Rayment, T. *Appl. Phys. Lett.* **1992**, *60*, 2356.
(39) Christenson, H. K.; Gruden, D. W. R.; Hong, R. G.; Israelachvili, J. N. *J. Chem. Phys.* **1987**, *87*, 1834.
(40) Winkler, R. G.; Schmid, R. H.; Gershmair, A.; Reineker, P. *J. Chem. Phys.* **1996**, *104*, 8103.

(41) Gupta, S.; Koopman, D. C.; Westermann-Clarke, G. B.; Bitsanis, I. A. *J. Chem. Phys.* **1994**, *100*, 8444.
(42) Rosenfeld, Y. *Phys. Rev. Lett.* **1989**, *63*, 980.
(43) Roth, R.; Evans, R.; Lang, A.; Kahl, G. *J. Phys.: Condens. Matter* **2002**, *14*, 12063.
(44) Yu, Y.-X.; Wu, J. *J. Chem. Phys.* **2002**, *117*, 1156.
(45) Sullivan, D. E.; Telo da Gama, M. M. In *Fluid Interfacial Phenomena*; Croxton, C. A., Ed.; Wiley: New York, 1986; p 45.
(46) Dietrich, S. In *Phase Transitions and Critical Phenomena*; Domb, C., Lebowitz, J. L., Eds.; Academic: London, 1988; Vol. 12, p 1.
(47) Vega, C.; Blas, F. J.; Galindo, A. *J. Chem. Phys.* **2002**, *116*, 7645.